Scattering of polarized ^{7}Li from ^{4}He

K. Rusek*
Department of Nuclear Reactions, The Andrzej Sołtan Institute for Nuclear Studies, Hoża 69, 00-681 Warsaw, Poland

P. D. Cathers,† E. E. Bartosz,‡ N. Keeley, K. W. Kemper, and F. Maréchal§
Department of Physics, The Florida State University, Tallahassee, Florida 32306-4350
(Received 7 October 2002; published 31 January 2003)

Complete sets of analyzing powers for elastic and inelastic (to the $1/2^-$ first excited and $7/2^-$ resonant states of ^{7}Li) scattering of polarized ^{7}Li by ^{4}He have been obtained. Relations between the different analyzing powers were determined by applying the invariant amplitude method. A comparison of these relations with the measured analyzing powers suggests that the odd rank tensor analyzing powers arise from higher order quadrupole interactions. The quadrupole interaction also gives rise to the inelastic analyzing powers. Continuum-discretized coupled-channels calculations using $\alpha+t$ cluster-folded potentials confirm this crucial role of the quadrupole interaction in producing the observed ^{7}Li+^{4}He analyzing powers. Cluster-folded spin-orbit and third rank tensor potentials were found to have negligible effects, in contrast to polarized deuteron elastic scattering where the spin-orbit potential plays the dominant role, even in producing the second rank analyzing powers. Coupling between the excited states of ^{7}Li, in particular that between the 0.478 MeV $1/2^-$ and the 6.68 MeV $5/2^-$ states, was also found to be important.

DOI: 10.1103/PhysRevC.67.014608 PACS number(s): 24.10.Eq, 24.70.+s, 25.70.Bc

I. INTRODUCTION

Recently [1] a complete set of elastic scattering observables for the spin 3/2 beam ^{7}Li scattered by a ^{4}He target was published. The data set consisted of angular distributions for the cross sections and first, second, and third rank analyzing powers at the two incident ^{7}Li energies of 31.5 and 45.5 MeV (11.45 and 16.55 MeV in the center of mass frame, respectively). The original goal of this work was to obtain a complete set of third rank analyzing powers so that a search could be made for the presence of a third rank tensor potential term in the optical model used to describe the scattering. The most striking experimental result was that the measured third rank analyzing power $^{T}T_{30}$ was found to be large at both energies, in contrast with the earlier ^{7}Li elastic scattering works by Tungate *et al.* [2] and Ott *et al.* [3] who measured $^{T}T_{30}$ for elastic scattering by heavier targets.

The data were analyzed in terms of the optical model with a phenomenological potential that consisted of central, spin-orbit, and second and third rank tensor terms. Triton exchange between the projectile and target was also included. The need for the presence of a third rank tensor potential term was inconclusive. Its inclusion in the analysis led to a worse description of the higher energy data and a better one of the lower energy data.

During the course of the elastic scattering data taking it was realized that the cross sections for exciting the ^{7}Li projectile were as large or larger than the elastic scattering for angles greater than 50°, suggesting that an analysis based on coupled−channels calculations would be needed to understand the data for the system ^{7}Li+^{4}He. The present work reports data for the excitation of ^{7}Li to its first excited 0.478 MeV $1/2^-$ state and to its 4.63 MeV $7/2^-$ second excited state. The latter state is 2.16 MeV above the $^{7}\mathrm{Li}\rightarrow\alpha+t$ breakup threshold. The data were obtained at the same energies and with the same experimental setup as the previously reported elastic scattering data [1], which results in a total of 54 angular distributions of nine observables.

The simultaneous analysis of these data within one model is a big challenge. One of the models that can be used and the one used here is that based on the continuum-discretized coupled-channels (CDCC) formalism [4]. This model allows the inclusion of effects due to projectile breakup to be explicitly included, which is important for projectiles with low breakup thresholds such as ^{7}Li. The cluster folding model was used to generate the interaction potentials from previously determined $t+^{4}$He and $\alpha+^{4}$He interactions. The emphasis in this work was to seek the origin of the observed analyzing powers and so all parameters needed for the calculations have been taken from other work.

The present paper is organized as follows. Section II contains a short description of the experimental procedure. Section III is devoted to predictions for the analyzing powers based on simple assumptions, while Sec. IV presents the coupled-channels methods used to understand the data. The results of the coupled-channels analysis are discussed in Sec. V, and the work is summarized in Sec. VI.

II. EXPERIMENTAL PROCEDURE

A detailed description of the elastic scattering measurements for the system ^{7}Li+^{4}He is given in [1]. The Florida State University tandem/linac accelerator system was used to obtain the scattering data. The cross sections were measured by scattering an α particle beam from a ^{7}Li target while the

*Electronic address: rusek@fuw.edu.pl
†Present address: University of Belize, Belize City, Belize.
‡Present address: CyTerra Corporation, Orlando, Florida.
§Present address: Institut de Recherches Subatomiques, BP28, F-67037 Strasbourg, Cedex 2, France.

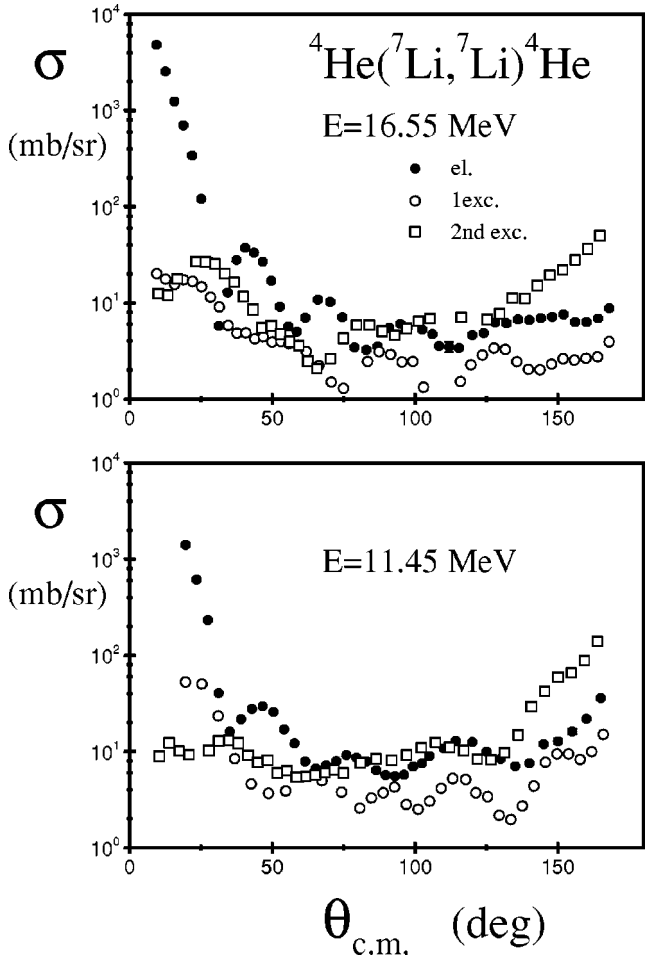

FIG. 1. Angular distributions of the cross sections for elastic scattering and inelastic scattering leading to the 0.478 MeV $1/2^-$ and 4.68 MeV $7/2^-$ states of ^{7}Li at $E_{\text{c.m.}}=11.45$ MeV and $E_{\text{c.m.}}=16.55$ MeV.

analyzing powers were measured by scattering a polarized ^{7}Li beam from a ^{4}He gas target made by filling a scattering chamber with natural He gas. It was possible to separate the first excited state at 0.478 MeV in ^{7}Li from the elastic peak in both sets of measurements by using relatively narrow detector collimators to limit the increase in peak width due to kinematic broadening. When scattering an α beam from a ^{7}Li target it is possible to extract inelastic cross sections over the whole angular range, whereas when using the polarized ^{7}Li beam it is only possible to extract analyzing powers for the unbound 4.63 MeV, $7/2^-$ state at the larger angles by observing the recoil α particles. When the ^{7}Li particles are detected, only the elastic and first excited state analyzing powers can be obtained. The measured elastic and inelastic scattering cross sections are shown in Fig. 1 for the two c.m. bombarding energies of 11.45 and 16.55 MeV. As can be seen, the inelastic scattering cross sections are as large as the elastic cross sections except for angles smaller than 50° c.m. The new inelastic scattering analyzing powers are presented in the figures that contain the results of the CDCC analysis throughout the rest of the text.

In this work the measured analyzing powers are presented

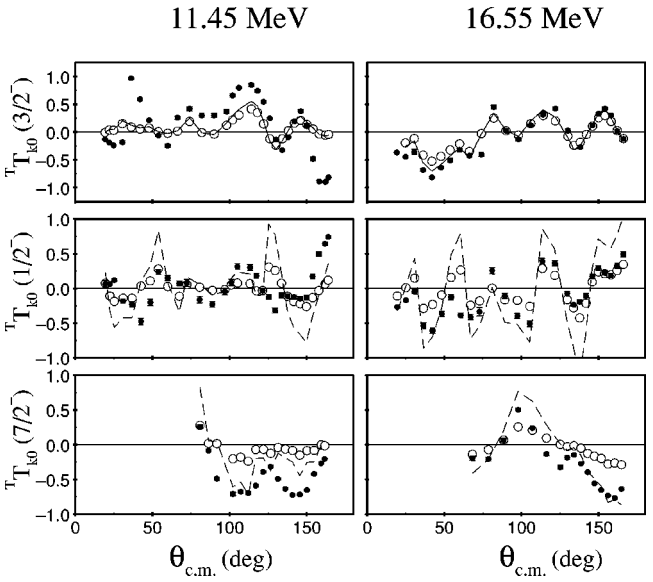

FIG. 2. Angular distributions of the vector and third rank tensor analyzing powers measured for ^{7}Li+^{4}He elastic ($3/2^-$) and inelastic scattering to the first excited state at $E_x=0.478$ MeV ($1/2^-$) and the resonant state at $E_x=4.68$ MeV ($7/2^-$). The solid circles denote the data for $^TT_{10}$ while the open circles denote the data for $^TT_{30}$. The solid curves represent the values of $^TT_{10}$ calculated for the elastic scattering according to Eq. (3) while the dashed curves denote those calculated for the inelastic scattering using Eq. (8).

in the Madison frame. However, in the derivation of relations between analyzing powers using the invariant amplitude method in the next section it is more convenient to work in the transverse frame for the odd tensor ranks. Use is made of two analyzing powers in the transverse frame, $^TT_{10}$ and $^TT_{30}$. They are related to the analyzing powers in the Madison frame by the following expressions:

$$^TT_{10}=\sqrt{2}iT_{11},$$

$$^TT_{30}=-\left(\sqrt{\frac{3}{4}}iT_{31}+\sqrt{\frac{5}{4}}iT_{33}\right).$$

III. INVARIANT AMPLITUDE PREDICTIONS FOR THE ANALYZING POWERS

A strong correlation between the vector, $^TT_{10}$, and the third rank tensor, $^TT_{30}$, analyzing powers was recently observed for the elastic scattering and t transfer reaction induced by polarized ^{7}Li on ^{12}C [5]. A simple explanation of this effect was given in the frame of the $\alpha+t$ cluster model of ^{7}Li. Bartosz *et al.* [5] concluded that, independent of the reaction, the angular distributions of both analyzing powers have the same zeros and the same sign between zeros if the process is in plane and if it is localized in the peripheral region of the two interacting nuclei.

In Fig. 2 angular distributions of $^TT_{10}$ and $^TT_{30}$ for elastic and inelastic ^{7}Li+^{4}He scattering measured for the two beam energies are compared. The solid circles represent data for the vector analyzing powers while the open circles correspond to the third rank tensor analyzing powers. They show

the correlation observed for the first time by Bartosz *et al.* [5] which suggests that these reactions are of a peripheral nature.

A. Elastic scattering

It has been demonstrated [6,7] that the invariant amplitude method [8] is very useful in studying polarization phenomena in nuclear reactions induced by polarized ^{7}Li ions. The method is based on the expansion of the transition matrix into amplitudes in accordance with the tensor rank in spin space. Amplitudes of different rank can be related directly to the analyzing powers. For example, if the amplitude U is a scalar, S is a vector, T_{2i} are the second rank tensors, and T_{3i} are the third rank tensors in spin space, then they represent the central, spin-orbit, second rank tensor, and third rank tensor interactions, respectively. Analyzing powers for the elastic and inelastic scattering of polarized ^{7}Li by a 0^+ target can be expressed in terms of these amplitudes [6,7]. In particular, by neglecting terms which include the third rank tensor amplitudes, the relations derived by Sakuragi *et al.* [6] for the elastic scattering reduce to

$$^{T}T_{10}=\frac{\sqrt{3}}{\sigma\sqrt{5}}\mathrm{Im}\left[\sqrt{\frac{1}{3}}US^{*}+\frac{2}{5}\sqrt{\frac{1}{3}}ST_{2a}^{*}+\frac{2}{5}ST_{2b}^{*}\right] \quad (1)$$

and

$$^{T}T_{30}=\frac{3}{10\sigma\sqrt{5}}\ \mathrm{Im}[ST_{2a}^{*}+\sqrt{3}ST_{2b}^{*}], \quad (2)$$

where σ is the cross section. Further, by neglecting the US^* term in Eq. (1) one obtains

$$^{T}T_{10}=\frac{4}{3}{}^{T}T_{30}. \quad (3)$$

This relation between the vector and third rank tensor analyzing powers is shown for the elastic scattering data in Fig. 2 by the solid curves. At the higher energy of 16.55 MeV this relation holds while at the lower energy of 11.45 MeV the data for the vector analyzing power are larger than calculated from the third rank tensor analyzing power data by means of Eq. (3). This means that at the lower energy the central and/or spin-orbit interactions must play a role in generating the analyzing power $^{T}T_{10}$ while at the higher energy the main source of the $^{T}T_{10}$ and $^{T}T_{30}$ analyzing powers is the quadrupole interactions.

By neglecting the U-independent terms in the relations derived by Sakuragi *et al.* [6] for the second rank tensor analyzing powers one gets

$$T_{22}\sin\theta=\sqrt{\frac{3}{2}}T_{20}\sin\theta+2T_{21}\cos\theta, \quad (4)$$

a simple formula that relates three second rank tensor analyzing powers for the elastic scattering. Here θ is the scattering angle. In Fig. 3, the values of the analyzing power T_{22} calculated in this way from the corresponding T_{20} and T_{21} data for the two incident energies are shown by the solid circles. The calculated values agree well up to a scattering angle of about 120° with the measured values shown by the open circles. The disagreement at large angles is not surprising as at backward scattering angles the contribution of the t-transfer reaction, indistinguishable experimentally from the elastic scattering, may be of importance.

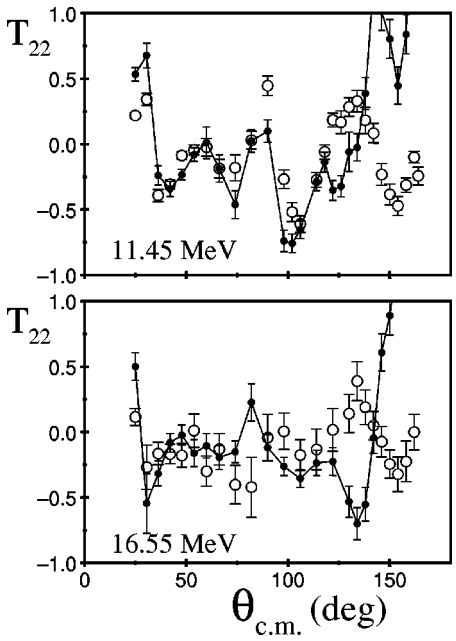

FIG. 3. Angular distributions of the second rank tensor analyzing power T_{22} for the elastic scattering of polarized ^{7}Li+^{4}He at the two incident energies. The open circles denote the experimental data while the solid circles were calculated from the experimental values for T_{20} and T_{21} using Eq. (4). The curves drawn through the solid circles are to guide the eye.

B. Inelastic scattering

Using the method of invariant amplitudes Sakuragi *et al.* [7] related the analyzing powers of all ranks for inelastic scattering of polarized ^{7}Li by a 0^+ target, leading to the first excited state of the projectile, with the corresponding amplitudes which represent different interactions. In particular, the vector and third rank tensor analyzing powers can be expressed as

$$^{T}T_{10}=\frac{1}{4\sigma\sqrt{5}}\ \mathrm{Im}[ST_{2b}^{*}+\sqrt{3}ST_{2c}^{*}-3\sqrt{3}T_{2a}T_{2b}^{*}+3T_{2a}T_{2c}^{*}], \quad (5)$$

$$^{T}T_{30}=\frac{1}{4\sigma\sqrt{5}}\ \mathrm{Im}[-3ST_{2b}^{*}-3\sqrt{3}ST_{2c}^{*}-\sqrt{3}T_{2a}T_{2b}^{*}+T_{2a}T_{2c}^{*}]. \quad (6)$$

If the S-dependent terms are dominant, one obtains

$$^{T}T_{10}=-\frac{1}{3}{}^{T}T_{30}, \quad (7)$$

and if the quadrupole interactions are more important than the spin-orbit interaction, then the relations reduce to

$$^{T}T_{10} = 3\,^{T}T_{30}. \tag{8}$$

Tungate *et al.* [9] proposed a simple model for the excitation of polarized ^{7}Li on a 0^{+} target, leading to the $1/2^{-}$ state of the projectile. They concluded that the odd rank tensor analyzing powers depend crucially on the excitation energy. Also, the third rank tensor analyzing powers are very sensitive to the spin transfer of one unit that may come from static or dynamic spin-orbit interactions. Moreover, if the process of inelastic scattering is dominated by the spin transfer of one unit, then the $^{T}T_{10}$ and $^{T}T_{30}$ analyzing powers fulfill Eq. (7), but if the quadrupole interactions are more important, these analyzing powers are related by Eq. (8), which confirms the findings of Sakuragi *et al.* [7].

Predictions obtained from Eq. (8) are shown with the experimental data for inelastic scattering of ^{7}Li+^{4}He for the two incident energies in Fig. 2. The dashed curves denote values of $^{T}T_{10}$ calculated from the $^{T}T_{30}$ experimental data by means of Eq. (8). In general, the calculated and measured values of the vector analyzing power are in good agreement for both the investigated excitations of ^{7}Li. This suggests that the quadrupole interactions play the dominant role in these inelastic processes.

Summarizing, comparison of the experimental data for elastic and inelastic scattering of polarized ^{7}Li by ^{4}He with the predictions using the relations of Refs. [5–7,9] leads to the conclusion that in all the experimental processes investigated here, the second rank tensor interactions must play a dominant role. The effects due to spin–orbit or third rank tensor interactions are of less importance. This is in contrast to polarized deuteron elastic scattering where the spin–orbit potential plays the dominant role, even in the determination of the second rank tensor analyzing powers [10].

IV. CDCC ANALYSIS

A. Cluster model of ^{7}Li and the cluster-folding interactions

In the CDCC analysis, the $\alpha+t$ model of ^{7}Li was applied. The $\alpha+t$ binding potential was that proposed by Buck and Merchant [11] and was of Gaussian form. Its parameters were determined from experimentally measured properties of ^{7}Li such as the rms radius of its charge distribution, its ground state spectroscopic quadrupole moment, its reduced transition probability for the excitation to its first excited state, $B(E2;3/2^{-}\rightarrow 1/2^{-})$, and its excitation energies. The parameters of the potentials used to calculate the cluster wave functions for the ground state, the first excited state at an excitation energy of 0.478 MeV, and the two resonant states at 2.16 MeV and 4.21 MeV above the $^{7}\mathrm{Li}\rightarrow\alpha+t$ breakup threshold are listed in Table I.

The cluster wave functions for the two resonant states were calculated using the CDCC method [4]. An energy bin width roughly corresponding to the empirical value was set for each of the two resonant states, and the wave functions calculated within the bins were averaged over the bin width. The wave functions derived in this way were normalized to unity. The depth of the binding potentials was varied in the course of the calculations to obtain resonances at the correct excitation energies.

TABLE I. Parameters of the $^{7}\mathrm{Li}=\alpha+t$ binding potentials, excitation energies, the widths of the energy bins used to generate the cluster wave functions as well as their quantum numbers for the ground state, the first excited state, and the two resonant excited states.

	V_0 (MeV)	V_{LS} (MeV)	R_0 (fm)	Shape	Ref.	NL	E_x (MeV)	ΔE_x (MeV)
$^{7}\mathrm{Li}_{3/2^-}$	83.780	1.003	2.52	Gauss	[11]	2P	0.00	0.00
$^{7}\mathrm{Li}_{1/2^-}$	82.940	1.003	2.52	Gauss	[11]	2P	0.478	0.00
$^{7}\mathrm{Li}_{7/2^-}$	84.940	1.003	2.52	Gauss	this work	1F	4.63	0.20
$^{7}\mathrm{Li}_{5/2^-}$	77.527	1.003	2.52	Gauss	this work	1F	6.68	2.00

In order to study the influence of the ^{7}Li breakup on the elastic and inelastic scattering, the $\alpha+t$ continuum above the breakup threshold was treated according to the model of Sakuragi *et al.* [4,6]. The continuum was discretized into momentum bins with respect to the momentum $\hbar k$ of the $\alpha-t$ relative motion. The width of most of the bins was set to 0.25 fm^{-1}. Two of the bins corresponding to states with spin-parity $7/2^{-}$ had different widths in order to avoid an overlap with the $7/2^{-}$ resonant state at excitation energy of 2.16 MeV above the breakup threshold. For each of the bins the geometry of the binding potential was kept fixed for the bound and resonant states, but their depth was different, depending on the relative orbital angular momentum L and spin J of the bin state. For the $L=0$, $J=1/2$ and $L=2$, $J=3/2$, 5/2 bin states as well as for the $L=1$, $J=3/2$ bins the depth of the binding potential was the same as for the ground state. For the $L=1$, $J=1/2$ bin states, the depth of the binding potential was taken to be the same as for the first excited state, while for the $L=3$ bin states the depth of the potential was the same as for the corresponding resonant states of the same spin J. The wave functions for the bin states were derived in the same way as for the resonant states, but they were not normalized to unity to avoid an artificial change of the wave function amplitudes at small separations between the clusters. The range of integration was set to 30 fm, which was found to be large enough for the final results of the analysis to be independent of this parameter.

All the diagonal and coupling potentials between the various states were derived from optical model $t+^{4}$He and $\alpha+^{4}$He potentials by means of the cluster-folding method [12]. A series of test calculations showed a strong dependence of the final results on the choice of these input potentials. Therefore, in this work the results of calculations with different sets of these potentials are presented.

The potentials were parametrized using the Woods-Saxon (WS) form

$$V(r) = \frac{V_{0,i}}{\exp\left(1+\dfrac{r-R_{0,i}}{a_{0,i}}\right)} \tag{9}$$

or the Gaussian form

TABLE II. Parameters of the input optical model potentials. Potential A is of a nonstandard form.

	V_0 (MeV)	R_0 (fm)	a_0 (fm)	V_i (MeV)	R_i (fm)	a_i (fm)	Shape	Ref.
$t+^4$He, A								[14]
$t+^4$He, B	87.00	1.80	0.70	10.00	1.80	0.70	WS	[13]
$t+^4$He, C	83.78	2.52	0.00	10.00	2.52	0.00	Gauss	[11]
$\alpha+^4$He, D	205.19	1.20	0.737	0.00	0.00	0.00	WS	this work
$\alpha+^4$He, E	125.00	1.78	0.66	0.00	0.00	0.00	WS	[17]
$\alpha+^4$He, F	122.62	2.132	0.00	0.00	0.00	0.00	Gauss	[18]

$$V(r) = V_{0,i}\exp\left[-\left(\frac{r}{R_{0,i}}\right)^2\right], \tag{10}$$

and are listed in Table II.

The $t+^4$He potential listed as set B is the potential calculated microscopically by Neudatchin *et al.* [13] with the exchange term neglected.

Another possible choice for the $t+^4$He optical model potential is to take the real potential of Buck and Merchant [11] that binds the two clusters into ^{7}Li and then add to it an imaginary term with the same geometry, but whose depth is varied to fit the experimental ^{7}Li$+^4$He elastic scattering cross section. The best results for both energies were obtained with a depth of 10 MeV and the full potential is listed as set C in Table II.

Recently, scattering of polarized ^{3}He from ^{4}He in the energy range from 20 MeV up to 30 MeV was studied and a potential consisting of central and spin-orbit terms was found [14]. The central term has two (complex) components of different geometries: an energy-dependent Wigner component and a Majorana component which depends strongly on the orbital angular momentum ℓ. This ℓ-dependence comes from the core (i.e., ^{3}He) exchange process. In this work, the Wigner component of the central potential for a ^{3}He energy of 20 MeV was used to generate the ^{7}Li$+^4$He cluster-folding interactions and is referred to as set A.

Calculation of the ^{7}Li$+^4$He potentials by means of the cluster–folding method at the two energies of 31.5 MeV and 45.5 MeV requires knowledge of the $\alpha+^4$He optical potentials at energies of 4/7 31.5$=$18 MeV and 4/7 45.5$=$26 MeV, respectively. There are experimental data for $\alpha+^4$He elastic scattering at an α bombarding energy of 23.1 MeV [15], close to that required. A fit to these data was obtained using the code ECIS79 [16], starting from the parameters proposed by Igo [15]. The potential obtained from this fit is listed in Table II as set D. We also used the potentials proposed by Kukulin *et al.* [17] and Buck [18] for this scattering system, listed as sets E and F, respectively, in Table II.

A spin-orbit potential for ^{7}Li$+^4$He can be derived within the cluster model from the empirical $t+^4$He spin-orbit interaction [12]. The elastic scattering of polarized tritons from ^{4}He has never been investigated: therefore, we used the potential found by Heiberg-Andersen *et al.* [14] for the elastic scattering of polarized ^{3}He from ^{4}He at an energy of 20 MeV. The potential has only a real component and it is not of a standard shape. It was parametrized in the following way:

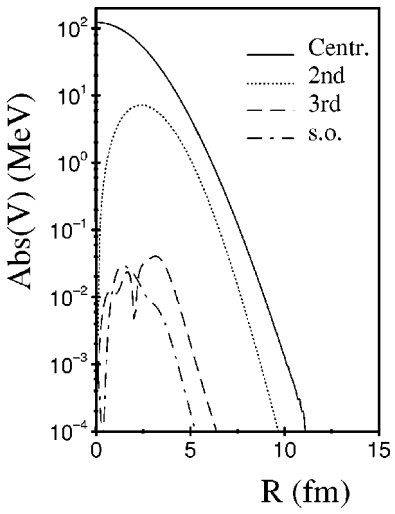

FIG. 4. The real parts of the cluster-folding potentials of different ranks for the ^{7}Li$+^4$He elastic scattering.

$$V_{\text{s.o.}}(r) = V_1\exp\left(-\frac{r^2}{a^2}\right) + V_2\exp\left[-\left(\frac{r-R}{b}\right)^2\right], \tag{11}$$

with parameters $V_1 = 4.1$ MeV, $V_2 = 0.82$ MeV, $R = 1.60$ fm, $a = 0.92$ fm, and $b = 1.00$ fm. We also used the spin-orbit potential found by Karban *et al.* [19] for the elastic scattering of polarized ^{3}He from ^{4}He at an energy of 33 MeV. Since the ^{7}Li$+^4$He spin-orbit potential calculated from the spin-orbit potential of Heiberg-Andersen *et al.* is stronger than that calculated from the potential of Karban *et al.*, calculations with these two potentials allow the role of the spin-orbit potential in producing analyzing powers to be investigated.

The second rank tensor potential was calculated according to the prescription given by Nishioka *et al.* [12] from the central t, α-target potentials C and F of Table II and from the t-target spin-orbit potential of Heiberg-Andersen *et al.* [14].

The third rank tensor potential corresponding to the transfer of the projectile spin $\Delta J = 3$ in the elastic scattering is also determined entirely by the t-target spin-orbit potential in the frame of the cluster model of ^{7}Li [12,20]. It was calculated from the same triton potential as the spin-orbit term. Since the original spin-orbit potential was real, the resulting spin-orbit and third rank tensor potentials were also real.

In Fig. 4 the real parts of the central, spin-orbit, second rank tensor, and third rank tensor potentials for the ^{7}Li $+^4$He elastic scattering calculated using central potentials C and F of Table II and the spin-orbit potential of Heiberg-Andersen *et al.* [14] are plotted. The spin-orbit and third rank tensor potentials are very weak, much weaker than the corresponding phenomenological potentials used in the optical model analysis of the same data sets [1]. They are also much weaker than the central or the second rank tensor cluster-folding potentials.

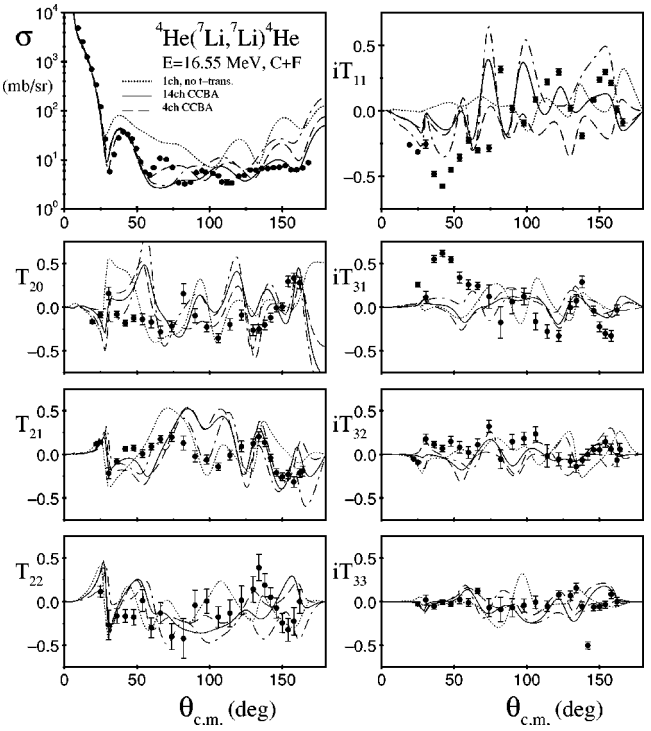

FIG. 5. Angular distributions of the differential cross section and analyzing powers of all ranks for elastic scattering of polarized ^{7}Li from ^{4}He at $E_{\mathrm{c.m.}}=16.55$ MeV. The curves show the results of coupled-channels calculations using cluster-folding potentials obtained from $t+^4$He potential set C and $\alpha+^4$He potential set F. The parameters of the potentials are listed in Table II. The dotted curves correspond to a one-channel calculation with the *t* transfer process omitted, the dashed curves to a four-channel calculation with the excited states of ^{7}Li listed in Table I included plus *t* transfer. The solid curves denote the results of the full 14-channel calculation which includes coupling to the $\alpha+t$ continuum in addition to the couplings included in the four-channel calculation. The dot-dashed curves denote the results of a similar 14-channel calculation with the transfer spectroscopic amplitude increased by a factor of 3.

B. Coupled-channels calculations

Diagonal and coupling interactions derived by means of the cluster-folding method were inserted into the coupled-channels code FRESCO [21], version FRXP.18. The coupled-channels calculations were performed for the two sets of data measured at center of mass energies of 11.45 and 16.55 MeV. All the parameters were kept fixed for calculations carried out at the two energies. In the coupled-channels calculations each bin was treated as an excited state of ^{7}Li, placed at an excitation energy equal to the mean energy of the bin. For the bound and resonant states of ^{7}Li, Nemets *et al.* [22] predicted the spectroscopic amplitudes to be very close to unity, so in the present work they were assumed to be equal to 1.0. Scattering wave functions were calculated at the mean energies of the bins and assumed to be energy independent within a bin.

A one-channel calculation was performed with the cluster-folding potentials of Fig. 4. The results are shown in Fig. 5 by the dotted curve for the ^{7}Li$+^4$He elastic scattering at 16.55 MeV. It was found that the contributions to the analyzing powers of the spin-orbit and the third rank tensor potential were negligibly small. All the calculated analyzing powers were generated by the second rank tensor potential. The large effect of the second rank tensor potential on the odd rank tensor analyzing powers for polarized ^{7}Li was first reported by Ohnishi *et al.* [23,24]. Although its contribution to the odd rank tensor analyzing powers must be a higher order effect [23], it was much larger than the first order contributions of the spin-orbit and third rank tensor potentials. This is almost exactly the opposite situation to polarized deuteron elastic scattering, where second order effects of the spin-orbit potential play a major role in generating the second rank tensor analyzing powers [10]. The one-channel calculation described well all the second rank tensor analyzing powers as well as iT_{32} and iT_{33}. The angular distributions of the differential cross section, vector analyzing power, and iT_{31} were not reproduced by the calculation. Since the coupling potentials of the first and third ranks between the various states in ^{7}Li, calculated by means of the cluster-folding method, are larger than the potentials of the corresponding ranks in the elastic channel, one may surmise that couplings to the excited states of ^{7}Li will improve the description of the vector and third rank tensor analyzing powers.

Test calculations were performed in order to check the dependence of the final results on the number of bins involved. They showed that the model space can be substantially reduced. Bin states with relative angular momentum $L=2,4$ were found to contribute very little to the final results. Also, bins with $L=1,3$ corresponding to the lowest mean excitation energy of 0.38 MeV above the breakup threshold were found to be unimportant. Therefore, most of the calculations were performed with ten bin states, two resonant states, and the two bound states of ^{7}Li. These are referred to as 14-channel calculations in what follows. The same coupling scheme was used by Kelly *et al.* [25] in the analysis of ^{6,7}Li breakup on ^{208}Pb.

Optical model analysis of the elastic scattering data [1] has shown that the process of triton transfer between the projectile and target improves the description of the large angle elastic scattering cross section but has little impact on the calculated analyzing powers. In this work *t* transfer leading to the ground, $1/2^-$ first excited and $7/2^-$ resonant states of ^{7}Li was included by means of the coupled-channels Born approximation (CCBA) method. To simplify the calculations, the same optical model potential was assumed for all three exit channels. For 11.45 MeV this was potential number 4 listed in Table I of Ref. [1], while for 16.55 MeV it was potential number 2. The tensor parts of these potentials were omitted. The final results depended very weakly on the choice of exit channel optical potential and were not sensitive to its tensor term. The transition potential for the *t* transfer was taken in the *post* form with a full complex remnant.

In the following, coupled-channels calculations with *t* transfer omitted are labeled CDCC, while those with *t* transfer included are labeled CCBA.

V. DISCUSSION

A. Sensitivity to optical potentials

The results of the calculations were found to depend strongly on the parameters of the input $t+^4$He and somewhat

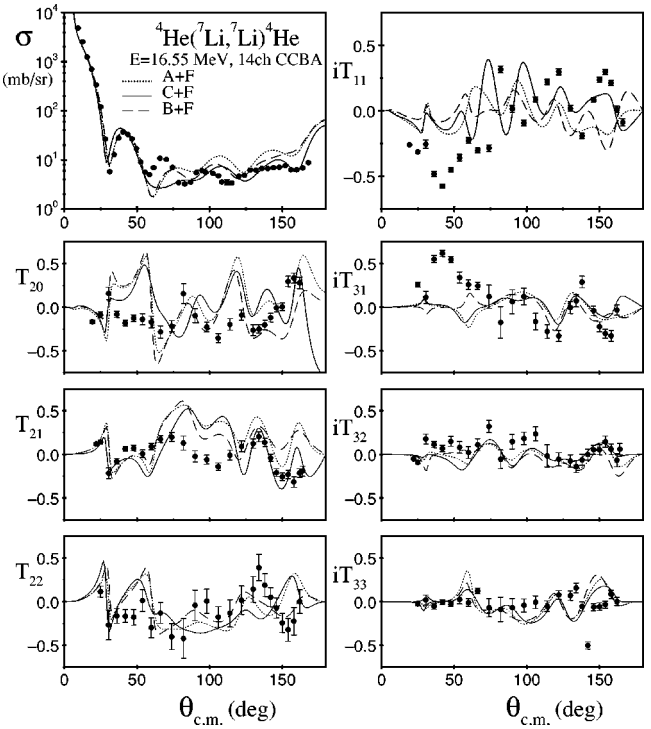

FIG. 6. Comparison of calculations for elastic scattering using cluster-folding interactions derived from $\alpha+^4$He potential C of Table II and the three different $t+$ ^{4}He optical potentials as discussed in the text.

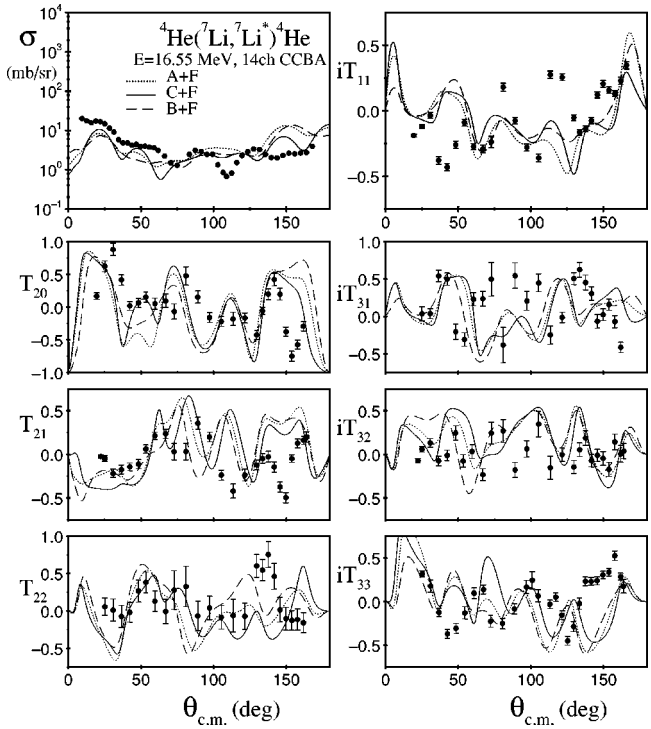

FIG. 7. As for Fig. 6, but for inelastic scattering leading to the $1/2^-$ first excited state of ^{7}Li.

more weakly on the $\alpha+^4$He optical model potentials used to generate the ^{7}Li$+^4$He cluster-folding interactions. In Figs. 6–9 the results of the 14-channel calculations with t transfer to the ground, $1/2^-$ first excited, and $7/2^-$ resonant states of ^{7}Li included at $E_{\text{c.m.}}=16.55$ MeV are shown. The calculations were performed with the cluster-folding interactions derived from $\alpha+^4$He potential F listed in Table II and each of the three $t+^4$He potentials A, B, and C. Comparison with the experimental data for elastic scattering and inelastic scattering leading to the $1/2^-$ first excited and $7/2^-$ resonant states of the projectile shows clearly that the details of the angular distributions cannot be described. Although the overall magnitudes of the calculated analyzing powers are similar to the measured values and the shapes of the calculated angular distributions are in many cases close to those observed experimentally, the details are poorly reproduced for many observables. The vector analyzing power was most sensitive to the $t+^4$He potential.

As a result of this potential sensitivity, the analysis focused on effects larger than the discrepancies due to the choice of $t+^4$He potential. There are angular ranges and observables where the predictions presented in Figs. 6–9 differ considerably from experiment. For elastic scattering at $E_{\text{c.m.}}=16.55$ MeV, the measured values of iT_{11}, iT_{31}, and $^TT_{30}$ at forward angles are much larger than the predictions. Although the calculation with $t+^4$He potential C closely reproduces the shape of the measured angular distribution for iT_{11} at forward angles, the calculated values are about 5 times smaller than the experimental ones. For inelastic scattering leading to the ^{7}Li $7/2^-$ resonance the measured iT_{31} angular distribution was not reproduced by the calculations, although the other analyzing powers are reasonably well described in the region for which data are available.

At the lower energy, $E_{\text{c.m.}}=11.45$ MeV, in contrast to the results at $E_{\text{c.m.}}=16.55$ MeV, the vector analyzing power for

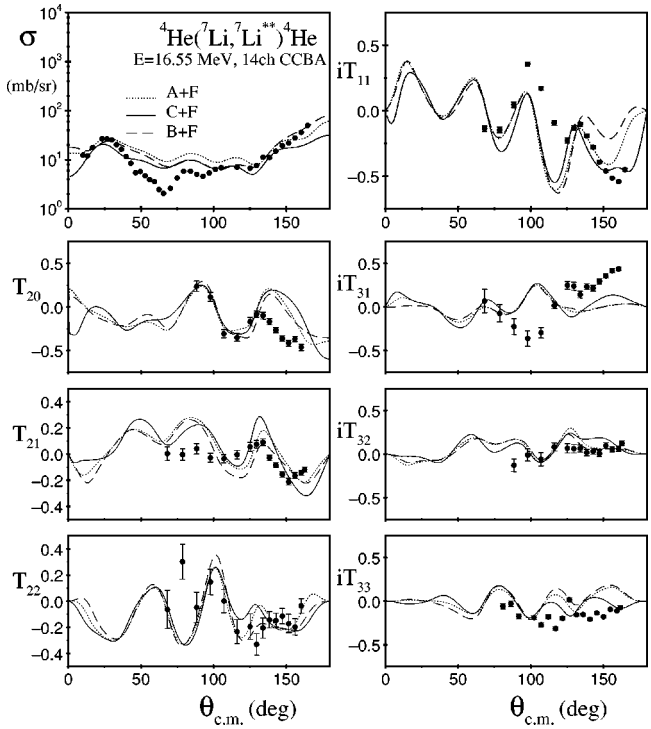

FIG. 8. As for Fig. 6, but for inelastic scattering leading to the $7/2^-$ resonant state of ^{7}Li.

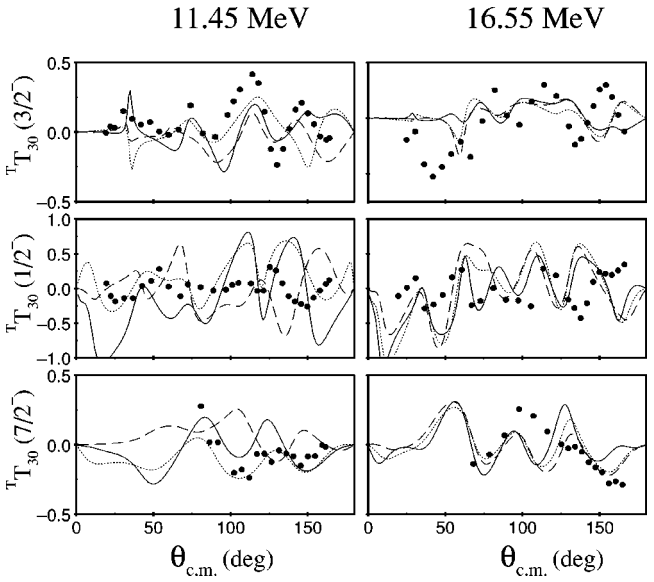

FIG. 9. Calculations as in Fig. 6 compared with the third rank tensor analyzing power $^{T}T_{30}$ at the two incident energies for elastic ($3/2^-$) and inelastic scattering leading to the first excited state of ^{7}Li at $E_x=0.478$ MeV ($1/2^-$) and the resonant state at $E_x=4.68$ MeV ($7/2^-$).

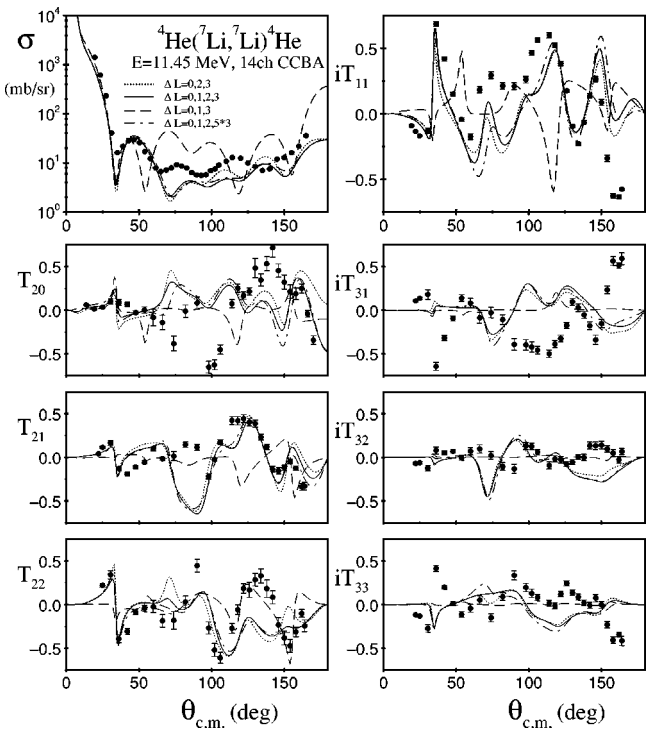

FIG. 10. Experimental data and results of coupled-channels calculations for ^{7}Li+^{4}He elastic scattering at $E_{c.m.}=11.45$ MeV. The solid curves denote the results of a 14-channel calculation which included t transfer. The results of a similar calculation with the strength of the octupole coupling potentials increased by a factor of 5 are denoted by the dot-dashed curves. Calculations with dipole couplings omitted are denoted by the dotted curves while calculations which omit quadrupole couplings are indicated by the dashed curves. All calculations were performed using cluster-folding interactions obtained from $t+$ ^{4}He potential C and $\alpha+^4$He potential F of Table II.

the elastic scattering was well reproduced by the calculations, including forward scattering angles (see Fig. 10). However, large discrepancies between the calculations and the data were again observed for iT_{31} for elastic scattering and inelastic scattering leading to the ^{7}Li $7/2^-$ resonance (see Fig. 12), the calculations giving much smaller values than experiment. Also, the description of the differential cross section angular distribution for inelastic scattering to the ^{7}Li $1/2^-$ first excited state was very poor, especially at forward scattering angles (see Fig. 11).

B. Effects of projectile excitation

Earlier analyses of polarized ^{7}Li scattering [12,23,24] reported large changes to the elastic scattering vector analyzing powers when coupling to the ^{7}Li excited states was included. This effect was also investigated in the present work. An example is shown in Fig. 5 for $E_{c.m.}=16.55$ MeV. One-channel calculations produced vector analyzing powers as a higher order effect of the second rank tensor potential. These results were significantly modified by the inclusion of projectile excitation to the three excited states listed in Table I. Inclusion of the $\alpha+t$ breakup states also changed the four–channel results. None of these effects, however, were able to produce the very large values of the vector analyzing powers at forward scattering angles around 50° observed in the experiment. At the lower energy, $E_{c.m.}=11.45$ MeV, 14-channel CCBA calculations reproduced well the angular distribution of the vector analyzing power including its large values at forward scattering angles, as shown in Fig. 10.

For inelastic scattering to the $1/2^-$ first excited and $7/2^-$ resonant states coupling to the $\alpha+t$ continuum reduced the calculated values of the differential cross section but analyzing powers of all ranks were not very sensitive to this coupling. They showed greater sensitivity to couplings to the bound and resonant excited states.

Coupling between the excited states of ^{7}Li was found to change the results of the calculations for all the observables. In particular, calculations which omitted couplings between the excited states produced much larger values of the differential cross section for inelastic scattering to the $1/2^-$ first excited state of ^{7}Li. This effect can be explained by the important role played by the coupling between the $1/2^-$ state and the $5/2^-$ resonance at an excitation energy of 4.21 MeV above the $\alpha+t$ breakup threshold. An example is given in Fig. 11 where the solid curves show the results of a 14-channel CCBA calculation. The dashed curves denote the results of a similar calculation which includes couplings to just the $1/2^-$ first excited and $7/2^-$ and $5/2^-$ resonant states. The results of this four-channel calculation are close to the full 14-channel results for all observables, showing that coupling to the continuum is not very important. However, the results of a similar four-channel calculation which omitted couplings between the excited states, denoted by the dotted curves in Fig. 11, are very different from the previous results. As the first excited state is not directly coupled to the $7/2^-$ resonance in our calculations the difference between the

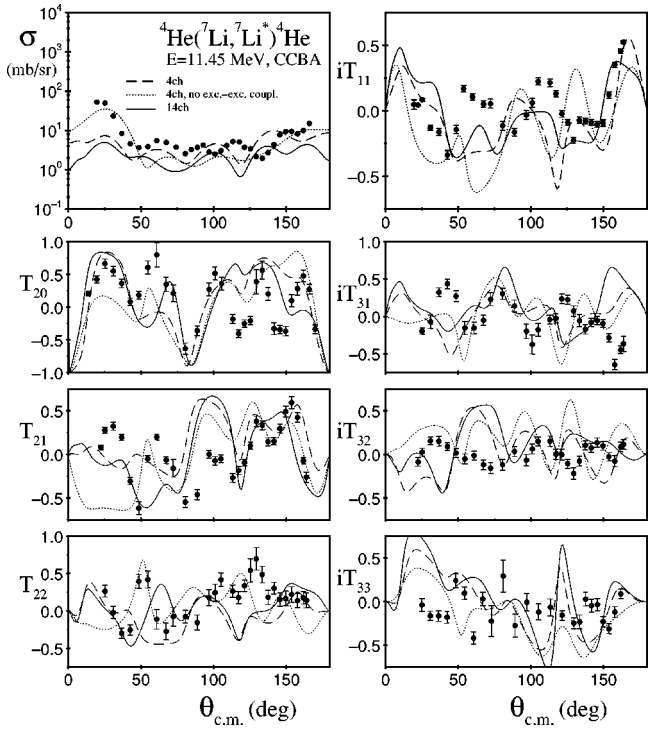

FIG. 11. Experimental data and results of coupled-channels calculations for ^{7}Li+^{4}He inelastic scattering at $E_{\mathrm{c.m.}}=11.45$ MeV leading to the first excited state of ^{7}Li. The solid curves denote the results of the full 14-channel CCBA calculation as in Fig. 10. The results of the four-channel CCBA calculation are shown by the dashed curves while the dotted curves denote the results of a similar four-channel calculation which omitted couplings between the excited states. The cluster-folding interaction used were the same as for Fig. 10.

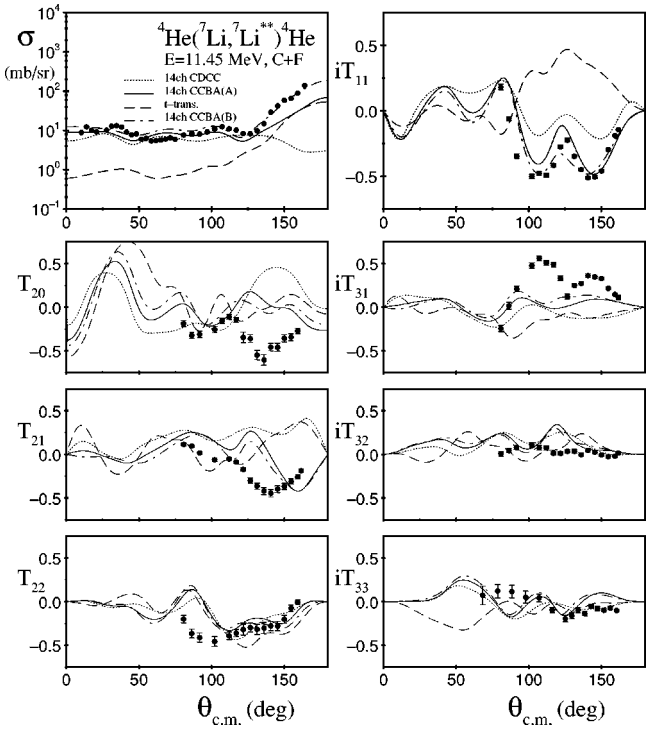

FIG. 12. Experimental data and results of coupled-channels calculations for ^{7}Li+^{4}He inelastic scattering at $E_{\mathrm{c.m.}}=11.45$ MeV leading to the $7/2^-$ resonant state of ^{7}Li at an excitation energy of 2.16 MeV above the $\alpha+t$ breakup threshold. The solid curves correspond to the full 14-channel CCBA calculation as in Figs. 10 and 11. The dashed curves denote the results for the *t*-transfer reaction while the dotted curves indicate the results of the CDCC calculation without *t* transfer included. The dot-dashed curves correspond to a 14-channel CCBA calculation with increased strength of the transfer component.

dashed and dotted curves is entirely due to the coupling to the $5/2^-$ resonance. A large effect due to coupling between the first excited state of ^{7}Li and the $5/2^-$ resonance was previously observed in the elastic scattering of polarized ^{7}Li from ^{26}Mg [3].

The role of different multipolarities ΔL of the couplings between various states of ^{7}Li was studied in the present work and the results are shown in Fig. 10. When $\Delta L=1$ couplings were omitted in the CCBA calculations the results at both energies were only slightly affected. To study the effects of $\Delta L=3$ couplings the model space was extended to include three bins corresponding to a relative cluster angular momentum of $L=4$ and spin $J=9/2$, placed between $k=0.25$ fm^{-1} and $k=1.0$ fm^{-1}. The effect of coupling to these states was also found to be negligible. However, large effects corresponding to the $\Delta L=2$ couplings were observed. When the quadrupole couplings were omitted the calculated values of the third rank tensor analyzing powers for the elastic scattering were reduced to very small values, as shown in Fig. 10 by the dashed curves. The vector and second rank tensor analyzing powers were also strongly affected. The T_{22} analyzing power exhibited the smallest sensitivity to the $\Delta L=2$ couplings. This was also true for inelastic scattering to the $7/2^-$ resonance. This can be explained by the fact that *t* transfer to the ground state and the $7/2^-$ resonance produces angular distributions for T_{22} that are very similar to those generated by the inelastic excitations.

C. Effects of the triton transfer process

Triton exchange between the projectile and the target was found in our earlier analysis of the ^{7}Li+^{4}He elastic scattering data [1] to be relatively unimportant. Its inclusion affected the differential cross section at backward scattering angles and this contribution was more important for the $E_{\mathrm{c.m.}}=11.45$ MeV data. The current work confirms this finding. Although the transfer itself produces very large analyzing powers of all ranks, it contributes to the scattering analyzing powers mainly at angles where the calculated cross section for transfer is comparable with the cross section for scattering. One exception to this rule was observed for the vector analyzing powers at $E_{\mathrm{c.m.}}=16.55$ MeV. The *t* transfer component contributed to the iT_{11} values at forward angles. A series of test calculations where the strength of the transfer component was artificially increased showed (the dot-dashed curves in Fig. 5) that the large measured values of iT_{11} can only be reproduced with an unphysically large spectroscopic amplitude. These test calculations also produced better

agreement with iT_{31} at forward angles, although in this case the effect is not so pronounced.

The calculated cross sections for t transfer to the ^{7}Li $7/2^-$ resonance were much larger than the cross sections for transfer to the ground state or the first excited state at both $E_{\text{c.m.}}=11.45$ MeV and $E_{\text{c.m.}}=16.55$ MeV. In Fig. 12 the dashed curves show the effect of t transfer to the $7/2^-$ resonance, the dotted curves the effect due to projectile excitation, and the solid curves the total results at $E_{\text{c.m.}}=11.45$ MeV. At scattering angles larger than 125° the measured values of the differential cross section are an order of magnitude larger than the CDCC results. When t transfer was included (the solid curves) this discrepancy was significantly reduced. The description of the iT_{11}, T_{20}, T_{21}, and iT_{31} analyzing powers was also improved. The other analyzing powers, in particular T_{22}, did not show such a sensitivity to the t transfer process. As the measured differential cross section at backward angles was still larger than the calculations, we performed CCBA calculations with an artificially increased t transfer spectroscopic factor. The results are shown in Fig. 12 by the dot-dashed curves. A similar effect to that produced by increasing the spectroscopic factor can be obtained by using a different $t+^4$He optical potential to calculate the cluster–folding interactions, as shown in Fig. 8.

For inelastic scattering leading to the first excited state of ^{7}Li the calculated cross section for t transfer was an order of magnitude smaller than for the $7/2^-$ resonance. Therefore, the effect of t transfer on this channel is small.

VI. SUMMARY

A large amount of experimental data, 54 angular distributions, were measured with very high precision for elastic and inelastic scattering of polarized ^{7}Li from ^{4}He at two ^{7}Li incident energies. Full sets of analyzing powers were obtained for the first time for inelastic scattering leading to the $1/2^-$ first excited and $7/2^-$ resonant states of ^{7}Li. Predictions based on simple models showed that the quadrupole interactions play a dominant role in all the experimentally investigated processes. These predictions were confirmed by large-scale coupled-channels calculations which included the effect of direct and sequential breakup of ^{7}Li into an α particle and a triton and which further included triton exchange between the projectile and target. All the parameters used in the calculations were derived from previous works on the scattering of tritons and α particles from ^{4}He as well as the cluster structure of ^{7}Li.

For the elastic scattering, the differential cross section and the vector analyzing power iT_{11} were found to be very sensitive to projectile excitation. Also, the triton exchange process between the projectile and target mostly affected these two observables. The second rank tensor analyzing powers T_{20} and T_{21} and the third rank tensor analyzing powers iT_{32} and iT_{33} originated mainly from the quadrupole reorientation of the ^{7}Li ground state. Quadrupole couplings to the excited states of ^{7}Li modified these results but not as much as for the vector analyzing power or cross section. The measured values of iT_{31} were larger than those of the other third rank tensor analyzing powers. At both incident energies they were poorly described by the calculations. The spin-orbit and third rank tensor potentials calculated by means of the cluster-folding model from the $t+^4$He spin-orbit potential did not have an important influence on the final results for any of the observables. Triton transfer and the choice of the $t+^4$He potential did not affect iT_{31} to any considerable extent. Coupled-channels calculations confirmed to some extent the strong correlation between the vector, $^TT_{10}$, and the third rank tensor, $^TT_{30}$, analyzing powers. At the lower energy $E_{\text{c.m.}}=11.45$ MeV, a good description of both these analyzing powers was achieved while at the higher energy $E_{\text{c.m.}}=16.55$ MeV, where the vector analyzing power was not well reproduced by the calculations, $^TT_{30}$ was also not well described.

The description of all the observables for inelastic scattering leading to the ^{7}Li $1/2^-$ first excited state was poor, especially for the data at $E_{\text{c.m.}}=11.45$ MeV. All the observables for this process were not very sensitive to the t transfer or couplings to the $\alpha+t$ continuum. They depended mainly on the reorientation of the ^{7}Li ground state and the coupling between the ground state and the first excited state and that between the first excited state and the $5/2^-$ resonance at an excitation energy of 4.21 MeV above the $\alpha+t$ breakup threshold.

In general, t transfer between the projectile and target is relatively unimportant. Its largest influence is on the inelastic scattering leading to the ^{7}Li $7/2^-$ resonance at an excitation energy of 2.16 MeV above the $\alpha+t$ breakup threshold. The large values for the vector analyzing power measured experimentally for this process originate from interference between the t transfer and inelastic excitation processes.

The question as to whether a third rank tensor potential is required to describe the third rank tensor analyzing powers could not be fully answered by the present work. Although the data were found to be insensitive to the third rank tensor interaction calculated using the cluster-folding model, the description of the data by the calculations is not good. In particular, the large values of the measured iT_{31} analyzing power obtained at forward angles for ^{7}Li$+^4$He elastic scattering at $E_{\text{c.m.}}=16.55$ MeV were not reproduced by the calculations and the origin of this discrepancy remains unclear.

Generally, comparison of the calculations and data suggests that the most interesting third rank tensor analyzing power for elastic scattering and inelastic scattering to the $7/2^-$ resonance is iT_{31}. This analyzing power is larger than either iT_{32} or iT_{33} and its description by the calculations caused the most serious problems. The analyzing powers iT_{32} and iT_{33} were found to be mainly sensitive to the quadrupole interaction generated by the ^{7}Li quadrupole deformation and, to a lesser extent, by projectile excitation.

Overall, the quality of the description of the experimental data by the large-scale coupled-channels calculations was determined in large part by our (lack of) knowledge of the $t+^4$He interaction. Some observables, such as the elastic scattering vector analyzing power, were very sensitive to the choice of the $t+^4$He interaction and the lack of a precise determination of this interaction at the required energies is a major handicap to our analysis.

Problems with the description of the data for inelastic

scattering to the ^{7}Li first excited state may point to a problem with the cluster model of ^{7}Li. All the observables for this process were found to depend on very few elements – the quadrupole couplings between the ground state, first excited state, and the $5/2^-$ resonant state of ^{7}Li.

In summary, we must conclude that the present data cannot be described using the best currently available models. Although we found that the results of these calculations were very sensitive to the choice of $t+^4$He optical potential, which is not known precisely enough, our analysis also indicates that the $\alpha+t$ cluster–folding model of ^{7}Li itself is not adequate to describe such data at bombarding energies well above the Coulomb barrier. In this energy regime clustering modes of ^{7}Li other than the $\alpha+t$ may be important, such as ^{6}Li$+n$ (threshold 7.25 MeV), ^{5}He+d (threshold 9.52 MeV), ^{6}He+p (threshold 9.98 MeV), etc. In order to include the effect of such clustering modes one would require an eight-body continuum calculation, for which a theoretical framework does not currently exist. Nevertheless, we were able to show the importance of quadrupole couplings in ^{7}Li in the generation of analyzing powers of all ranks, even if the agreement with data is more qualitative than quantitative. These data evidently provide a severe test for models of ^{7}Li and will prove a challenge for more sophisticated many-body continuum calculations that may be devised in the future.

ACKNOWLEDGMENTS

The authors would like to thank Dr. H. Heiberg-Andersen for making available his ^{3}He$+^4$He potentials prior to publication. This work was supported by the U.S. National Science Foundation, the State of Florida, and NATO, Grant No. PST.CLG.978953.

[1] P.D. Cathers, E.E. Bartosz, M.W. Cooper, N. Curtis, N. Keeley, K.W. Kemper, F. Maréchal, E.G. Myers, B.G. Schmidt, K. Rusek, and V. Hnizdo, Phys. Rev. C **63**, 064601 (2001).
[2] G. Tungate, D. Krämer, R. Butsch, O. Karban, K.-H. Möbius, W. Ott, P. Paul, A. Weller, E. Steffens, K. Becker, K. Blatt, D. Fick, B. Heck, H. Jänsch, H. Leucker, K. Rusek, Irena M. Turkiewicz, and Z. Moroz, J. Phys. G **12**, 1001 (1986).
[3] W. Ott, R. Butsch, H.J. Jänsch, K.-H. Möbius, P. Paul, K. Rusek, Z. Moroz, I.M. Turkiewicz, K. Becker, K. Blatt, H. Leucker, and D. Fick, Nucl. Phys. **A489**, 329 (1988).
[4] Y. Sakuragi, M. Yahiro, and M. Kamimura, Prog. Theor. Phys. Suppl. **89**, 136 (1986).
[5] E.E. Bartosz, P.D. Cathers, K.W. Kemper, F. Maréchal, D. Robson, G. Grawert, and K. Rusek, Phys. Lett. B **488**, 138 (2000).
[6] Y. Sakuragi, M. Yahiro, M. Kamimura, and M. Tanifuji, Nucl. Phys. **A462**, 173 (1987).
[7] Y. Sakuragi, M. Yahiro, M. Kamimura, and M. Tanifuji, Nucl. Phys. **A480**, 361 (1988).
[8] M. Tanifuji and K. Yazaki, Prog. Theor. Phys. **40**, 1023 (1968).
[9] G. Tungate, S.J. Hall, J. Gomez-Camacho, and R.C. Johnson, J. Phys. G **18**, 367 (1992).
[10] H. Nishioka and R.C. Johnson, Nucl. Phys. **A440**, 557 (1985).
[11] B. Buck and A.C. Merchant, J. Phys. G **14**, L211 (1988).
[12] H. Nishioka, J.A. Tostevin, R.C. Johnson, and K.-I. Kubo, Nucl. Phys. **A415**, 230 (1984).
[13] V.G. Neudatchin, V.I. Kukulin, A.N. Boyarkina, and V.P. Korennoy, Lett. Nuovo Cimento **5**, 834 (1972).
[14] H. Heiberg-Andersen, R.S. Mackintosh, and J.S. Vaagen, Nucl. Phys. **A713**, 63 (2002).
[15] G. Igo, Phys. Rev. **117**, 1079 (1960).
[16] J. Raynal, Computer code ECIS79, (unpublished).
[17] V.I. Kukulin, V.G. Neudatchin, and Yu. F. Smirnov, Nucl. Phys. **A245**, 429 (1975).
[18] B. Buck, Nucl. Phys. **A275**, 246 (1977).
[19] O. Karban, A.K. Basak, C.O. Blyth, W. Dahme, J.B.A. England; J.M. Nelson, N.T. Okumusoglu, S. Roman, G.G. Shute, and R. Vlastou, J. Phys. G **3**, 571 (1977).
[20] D. Mukhopadhyay, G. Grawert, D. Fick, and Z. Moroz, Phys. Lett. **104B**, 361 (1981).
[21] I.J. Thompson, Comput. Phys. Rep. **7**, 167 (1988).
[22] O.F. Nemets, V.G. Neudatchin, A.T. Rudchik, Yu. F. Smirnov, and Yu. M. Tchuvil'ksii, *Nucleon Clusters in Atomic Nuclei and Many-Nucleon Transfer Reactions* (Ukrainian Academy of Sciences, Institute for Nuclear Research, Kiev, 1988).
[23] H. Ohnishi, M. Tanifuji, M. Kamimura, and M. Yahiro, Phys. Lett. **118B**, 16 (1982).
[24] H. Ohnishi, M. Tanifuji, M. Kamimura, Y. Sakuragi, and M. Yahiro, Nucl. Phys. **A415**, 271 (1984).
[25] G.R. Kelly, N.J. Davis, R.P. Ward, B.R. Fulton, G. Tungate, N. Keeley, K. Rusek, E.E. Bartosz, P.D. Cathers, D.D. Caussyn, T.L. Drummer, and K.W. Kemper, Phys. Rev. C **63**, 024601 (2001).